A compliant-mechanism-based three degree-of-freedom manipulator for small-scale manipulation
John Speich and Michael Goldfarb

Department of Mechanical Engineering, Vanderbilt University, Box 1592, Station B, Nashville, TN 37235 (USA)

SUMMARY
This paper describes the design of a small-scale three degree-of-freedom compliant-mechanism-based manipulator with an approximately 2 cm × 2 cm × 2 cm cubic workspace. The manipulator exhibits a significantly larger range of motion and better spatial structural properties than a conventional compliant mechanism, due primarily to a unique flexure joint developed by the authors. A brief description of the mechanics of the flexure joint is followed by a description of the design of the manipulator. Following the mechanical description, the design of the low-level manipulator controller is discussed. Finally, data is presented that demonstrates manipulator performance.

KEYWORDS: Compliant mechanism; Flexure joint; Manipulator controller; Small-scale manipulation.

1. INTRODUCTION
Though considerable research has been directed toward the advancement of robotic manipulation on a conventional scale (i.e. millimeters to meters), relatively little work has been conducted on robotic manipulation at a microscopic scale (i.e., microns to millimeters). Once developed, interactive micromanipulator technology will have application in many fields, including micromanufacturing, microsurgery, telesurgery, microbiology and pharmaceutical research. Many microscale parts, for exmaple, have been fabricated utilizing photolithographic and X-ray lithographic microfabrication techniques. Despite these advanced microfabrication techniques, widespread commercial availability of multi-element microelectromechanical (MEMS) devices (e.g. a MEMS gearbox) has not yet come to fruition, due in part to the difficulty entailed in assembling the very small parts, and in particular to assemble in large quantities (i.e. mass produce). A micromanipulator would enable dexterous handling of micromanufactured parts, and thus enable the assembly and production of functional multi-element MEMS devices. If utilized in a teleoperative sense, a conventional-scale manipulator master coupled to a small-scale manipulator slave could enable dexterous human-controlled telemanipulation of a small-scale environment. In this sense, the telemanipulation system would address human positioning limitations in the forward path and limited human force sensitivity in the backward path. Coupled with a stereomicroscope, this technology would enable dexterous interaction between a human and a microscopic environment.

2. DESIGN SPECIFICATIONS FOR MICROASSEMBLY
As previously described, one of the principal purposes of a micromanipulator is for microassembly (e.g. the assembly of MEMS). Such tasks are enhanced significantly by a manipulator with an adequately sized workspace and a reasonable large bandwidth. Additionally, the ability of a manipulator to perform small-scale assembly tasks is improved considerably by a device that is capable of a widely variable output impedance and by a device that is devoid of hard nonlinearities. In particular, these characteristics have important implications with respect to the ability of a manipulator to perform small-scale assembly tasks in a stable and accurate manner as described in the following two sections.

2.1 Variable output impedance
Several commercially available micro-positioning systems exist to perform micro positioning tasks, such as PZT-based stages and electromagnetic motor and ball-screw based devices. Such devices work well for pure positioning tasks, but are not well suited for assembly, which is a manipulation rather than a positioning task. Specifically, an important distinction exists between manipulation and positioning, which has particular significance when considering the closed-loop stability of a device. The objective of a positioning task is essentially to ignore kinematic constraints in the environment (i.e. the notion of disturbance rejection), while the objective of a manipulation tasks is generally to utilize kinematic constraints in the environment to guide the manipulator motion. In order to achieve this, a manipulation task generally requires some combination of position and force control (i.e. position/force hybrid, admittance, impedance, etc). Controlling force against a kinematic constraints (i.e. a high environment impedance) in turn requires that the manipulator exhibit a low output impedance along the instantaneous axis (or axes) of force control. Specifically, as described by An and Hollerbach,[1] Colgate and Hogan,[2] Eppinger and Seering,[3] and Kazerooni,[4] significant closed loop stability problems exist when both the (input) impedance of the environment and the

(output) impedance of the manipulator are large, since in such cases, small perturbations in motion generate large changes in force. Applications that involve closed-loop force control in the presence of high or variable environment impedances (e.g. assembly tasks) are therefore best served with devices that are capable of a low output impedance, which in turn provide stable manipulator behavior. Such applications should not therefore be addressed with non-backdrivable, high output impedance devices, but rather should be addressed with variable output impedance (backdrivable) devices.

2.2 Minimizing hard nonlinearities

Operation in small-scale, often delicate environments requires stable and precise control of manipulator motion. One of the most significant impediments to effective implementation of precision control in micromanipulation is the presence of hard nonlinearities, in particular backlash and Coulomb friction, in the open loop manipulator mechanics.[5–9] The study of (convention-scale) direct-drive robots was borne out of the necessity to implement precision position control of robot manipulation for purposes of mechanical interaction, since a direct-drive design significantly reduces the amount of backlash and Coulomb friction in the manipulator.[10]

Due to the physics of scaling, devices that operate on a microscopic scale are influenced by highly nonlinear surface forces to a much greater degree than those of a conventional scale.[11–13] Conventional-scale manipulator behavior is typically dominated by inertial effects, which are fundamentally smooth and tend to filter the effects of hard nonlinearities on manipulator motion. The significance of inertial mechanics, however, diminishes with decreasing scale. The magnitude of inertial forces is typically in proportion to volume (assuming invariance of density), and thus scales with the cube of the geometric scaling ratio. Since friction is a surface force, its magnitude scales conservatively in proportion to surface area, and thus scales with the square of the geometric scaling ratio. Geometrically similar but small devices therefore exhibit increased surface effects and decreased inertial effects. The problem with this increase is that interaction dominated by friction forces is far more difficult to control than that dominated by inertial forces. Inertial forces are fundamentally smooth, while friction forces, especially those present during sliding, are typically highly nonlinear (e.g. stick-slip phenomena) and quite difficult to control. The net effect of surface-force-dominated behavior is severe deterioration of position and/or force control. If Coulomb friction is independent of surface area, as the conventional conception suggests, then the increased ratio of frictional to inertial effects at decreasing scales is even greater. Consequently, a small-scale manipulator that is fabricated as a scaled-down version of a conventional scale robot will exhibit a significantly greater (relative) amount of Coulomb friction, and thus exhibit degraded performance (relative to the conventional scale). The precision control of a small-scale manipulator will therefore be significantly enhanced by design approaches that minimize hard nonlinearities such as

backlash and Coulomb friction in the manipulator mechanics.

3. SURVEY OF MANIPULATOR DESIGNS

Several approaches have previously been or are currently being taken to the design of a small-scale precision manipulator. Hunter et al.[14,15] developed a micro-robot that incorporates three types of actuators arranged in series to provide motion: linear electromagnetic motors and micro-stepper motors for large scale motion and piezoelectric slabs for very small movements. Hannaford et al.[16] developed a direct-drive mini-robot for teleoperation purposes which is essentially a scaled-down direct-drive conventional-scale robot that utilizes DC motors as actuators. Colgate et al.[17] developed a device that incorporates a six degree-of-freedom Stewart platform actuated by DC servomotors that drive linear slides through ballscrew transmissions. Hollis and Salcudean have developed an innovative actuator based on Lorentz forces for the purpose of fine motion robotics, and have incorporated into it a telemicrorobotic system.[18–21] The six degree-of-freedom levitated system provides a workspace of approximately $4 \text{ mm} \times 4 \text{ mm} \times 3 \text{ mm}$ in translation and $\pm 4° \times \pm 4° \times \pm 10°$ in rotation. Fukuda et al.[22] designed a piezoelectric ceramic-driven six degree-of-freedom compliant mechanism microrobot. Since the robot does not incorporate significant amplification of the piezoelectric actuator displacement and does not include any other means of actuation, the total range of motion of the manipulator endpoint is approximately fifty microns and has an achievable total rotational range of 0.27 degrees. Kallio et al.[23] have developed a three degree-of-freedom piezohydraulically actuated manipulator, which utilizes a hydraulic transmission to amplify piezoelectric motion to enable a workspace of $1.5 \text{ mm} \times 0.6 \text{ mm} \times 0.25 \text{ mm}$. Another research effort, which due to private investment has remained relatively unpublished, is that of Charles et al.[24] This device is a cable-driven revolute joint based five degree-of-freedom manipulator.

All of these approaches have at least one detriment for the purpose of small-scale assembly. The manipulators of Hunter et al., Hannaford et al., Colgate et al., and Charles et al. (which were developed primarily for positioning tasks) are in essence scaled-down versions of conventional design approaches (i.e. they contain conventional roller bearings and similar design components), and thus exhibit an increased proportion of frictional to inertial effects (relative to the conventional scale). Additionally, the manipulator of Colgate et al. exhibits high output impedance and would most likely not be appropriate for high impedance environments. The manipulators of Fukuda et al., Hollis and Salcudean, and Kallio et al. depart from conventional design and eliminate friction, but offer small ranges of motion.

This paper describes the development of a small-scale manipulator that enables a significant range of motion and bandwidth in a device that is essentially devoid of frictional effects and is capable of a widely variable output impedance. Specifically, the manipulator described in the paper is a three-degree-of-freedom spatial compliant mechanism that is based upon a unique flexure-based revolute joint developed by the authors.

4. COMPLIANT MECHANISM DESIGN

The adverse effects of hard nonlinearities on the performance of robot manipulation can be avoided by designing compliant-mechanism-based "smooth" manipulators. A compliant mechanism is a device that moves solely by deformation, typically by utilizing flexures in place of conventional bearings. Since these devices do not entail any sliding or rolling, they are free of backlash and Coulomb friction, and thus have perfectly smooth mechanics. In addition to significantly enhancing control stability, the absence of hard nonlinearities in compliant mechanism behavior places no fundamental physical limitations on the resolution of position or force control.

Movement of a compliant mechanism can be a result of distributed compliance, but more commonly incorporates rigid links and lumped compliances at flexible joints. Specifically, a typical compliant mechanism utilizes flexure joints in place of the conventional revolute joints utilized in conventional mechanism design. A standard revolute flexure joint, such as those universally described in the compliant mechanism literature,[25–29] is based upon the bending deflection of cantilever beams. In contrast, the standard revolute joint in a conventional mechanism is based upon the sliding or rolling of a journal or rolling element bearing. A conventional flexure and a standard revolute joint are depicted in Figure 1. An example of a compliant mechanism that incorporates conventional bending-beam flexure joints is the small-scale robot gripper shown in Figure 2. This mechanism, developed by Goldfarb and Celanovic,[30] contains twelve revolute flexure joints and approximates the linkage shown in Figure 3.

4.1 Advantages of compliant mechanisms
Compliant mechanisms offer several significant advantages relative to conventional mechanisms. Perhaps the most
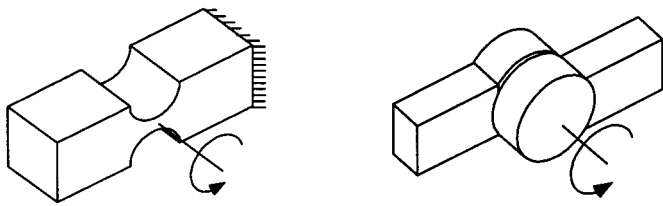

Fig. 1. Diagram of a conventional flexure and a standard revolute joint, indicating the nominal joint axis of rotation.
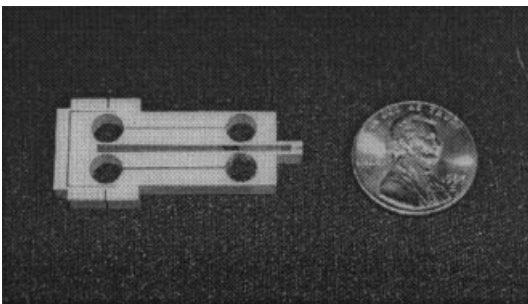

Fig. 2. Small-scale robot gripper as an example of a compliant mechanism that incorporates conventional bending-beam flexure joints.
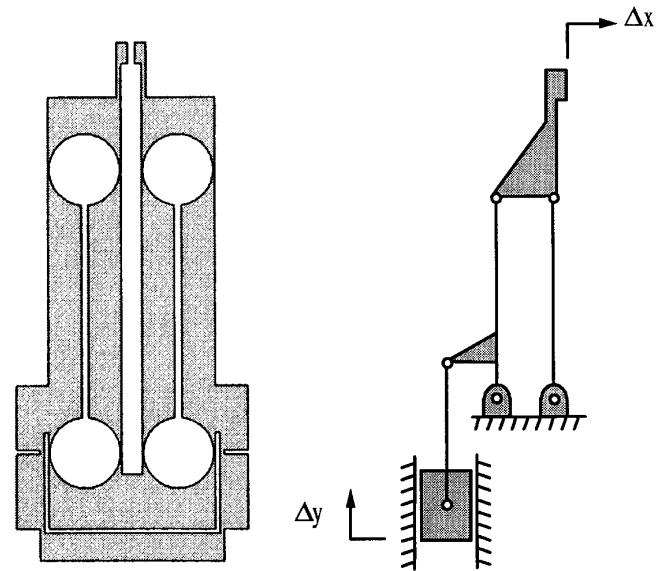

Fig. 3. Two-dimensional drawing of the gripper structure and the kinematically idealized schematic of (one half of) the flexure-based linkage.

notable of these is the absence of Coulomb friction and backlash, two behaviors that impede the performance of precision mechanisms. Typical mechanisms which incorporate conventional journal or rolling element bearings exhibit some degree of both backlash and Coulomb friction. The backlash can often be eliminated by applying a bias load (or preload) to the bearings, but utilizing such a load increases Coulomb friction, and as such eliminates one adverse behavior in exchange for another. Since compliant mechanisms are devoid of backlash and Coulomb friction, they are well suited to precision mechanism design, and are often utilized as such. In addition to eliminating friction and backlash, compliant mechanisms are free of lubricants, and thus are extremely conducive to clean environments.

4.2 Disadvantages of compliant mechanisms
Though compliant mechanisms eliminate Coulomb friction and backlash from a device, they also have several deficiencies relative to a conventional mechanism. Flexure pivots have a limited range of motion, depending on the geometry and material properties. In contrast, a typical conventional revolute joint has an infinite range of motion. Another significant problem with conventional flexures is the poor structural properties exhibited when subjected to multi-axis loading. An ideal revolute joint is infinitely rigid in all directions of loading except about the desired axis of rotation. In contrast, a conventional flexure exhibits a significant stiffness along the desired axis of rotation and significant compliance along all other axes of loading. A flexure-based joint, for example, will twist when subjected to torsional loads and exhibit shear deformation when subjected to shear loads, as illustrated in Figure 4. Finally, compliant mechanisms constructed of conventional cantilever-type flexure joints exhibit non-ideal kinematic behavior. Specifically, unlike a conventional revolute joint, a cantilever-type flexure joint does not have a fixed axis of rotation. Rather, the axis of rotation of a cantilever-type flexure joint
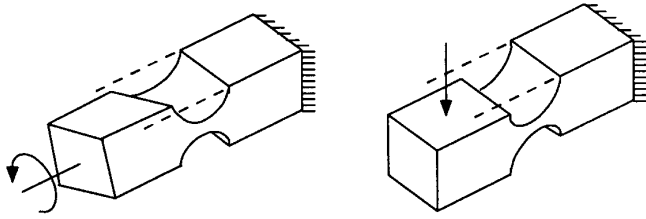
Fig. 4. Torsional and shear deformation of a conventional flexure joint.

(i.e. the instant center of rotation of one link relative to the other) will move along a locus of points in the vicinity of the joint as the joint flexes. The kinematic deficiencies are particularly significant in applications requiring accurate kinematic transformations, such as controlling the endpoint of a manipulator when sensing displacement in the joint space.

4.3 Split-tube flexure
The authors have developed a new type of flexure that exhibits a considerably larger range of motion and significantly better multi-axis structural properties than a conventional flexure. The design of the joint is based upon contrasting the torsional compliance of an open section with its stiffness in compression and bending. The torsional mechanics of closed section and open section members are fundamentally and significantly different, while the bending and compressive mechanics of the members are quite similar. This difference in mechanics enables minimizing of torsional stiffness and maximization of all other stiffnesses in a nearly decoupled manner. Figure 5 shows two hollow shafts that are in every manner identical except that one has a slit along its long axis. Though geometrically similar, the mechanics of how each bears a torsional load are quite different. For purposes of torsional mechanics, the wholly intact shaft reacts mechanically in the same mode as a solid shaft, while the slitted shaft behaves mechanically as a thin flat plate. This dissimilarity in behavior results in very different torsional stiffnesses.

Defining torsional stiffness as the ratio of torque about the long axis to the angular deflection about the same, a simple analysis illustrates the differences in torsional mechanics. Assuming typical properties such as linearly elastic, homogeneous, and isotropic material, the torsional stiffness of the closed section, k_c, is given by:

$$k_c = \frac{GJ}{L} = \frac{G}{L}\frac{\pi}{2}[R^4 - r^4] = \frac{G}{L}\frac{\pi}{2}[R^4 - (R-t)^4]$$
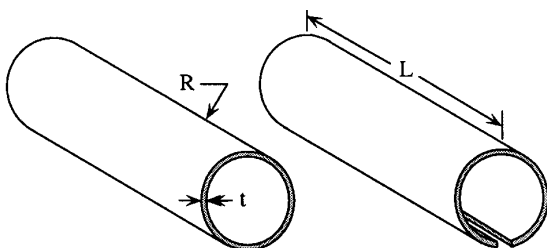

Fig. 5. Closed and open section hollow shafts.

$$= \frac{G}{L}\frac{\pi}{2}[4R^3t - 6R^2t^2 + 4Rt^3 - t^4] \tag{1}$$

where G is the shear modulus of elasticity, and L, R, r, and t are the length, outside radius, inside radius and wall thickness of the shaft, respectively. Since by definition, the geometry of a thin-walled shaft is such that $t \ll R$, the first term of the right hand side can be neglected, and therefore the torsional stiffness of the closed section can be written as:

$$k_c \approx \frac{2\pi G}{L}R^3 t \tag{2}$$

The open section stiffness, K_o can be obtained via the use of the membrane analogy[31] and is given by:

$$k_o = \frac{2\pi G}{3L}Rt^3 \tag{3}$$

The resulting ratio of the open section to the closed section stiffness can be written:

$$\frac{k_o}{k_c} \approx \frac{1}{3}\left(\frac{t}{R}\right)^2 \tag{4}$$

Since by definition, the geometry of a thin-walled shaft is such that $t \ll R$, the torsional stiffness of the open section is significantly less than that of its closed counterpart. For example, a closed-section shaft of radius $R = 2.5$ mm and wall thickness $t = 0.05$ mm would exhibit a torsional stiffness approximately 7500 times that of a geometrically similar open section.

Though the torsional mechanics of the open and closed section shafts are quite different, the mechanics of bending are in essence the same. Defining the bending stiffness as the ratio of applied moment to angular deflection and assuming the opening in the open section is small, both open and closed section shafts have a bending stiffness given by:

$$k_b = \frac{\pi E}{L}R^3 t \tag{5}$$

where E is the modulus of elasticity, and the other variables are as defined previously. Note that this stiffness is quite similar to the torsional stiffness of a closed section shaft. In fact, in the limit of $t \ll R$, the joint structure would have a zero torsional stiffness and an infinite bending stiffness, emulating the ideal revolute joint without the corresponding backlash and Coulomb friction. This, in essence, characterizes the design of the split-tube flexure. Figure 6 shows photographs of a split-tube flexure hinge. Note that the axis of rotation is along the bottom of the tube opposite the split, and not through the center of the tube.

A previously-published comparison between the split-tube flexure and a conventional flexure showed that, for a given geometry, the split-tube flexure exhibits a range of motion more than five times larger, off-axis stiffnesses three to four orders of magnitude larger, and maximum loads
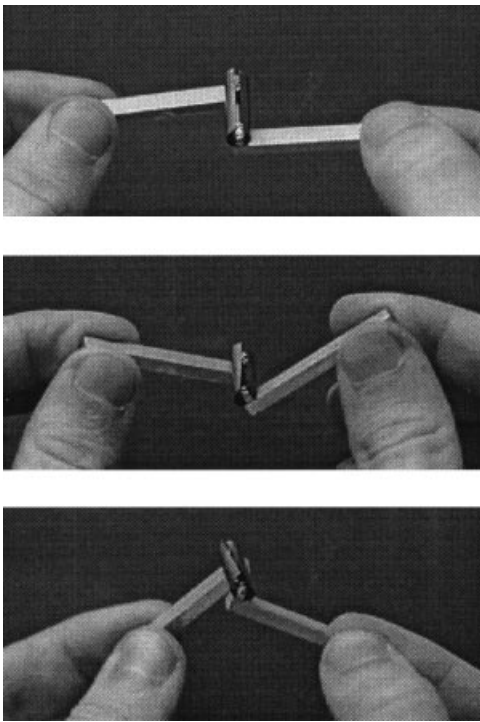
Fig. 6. Split-tube flexure revolute joint.

approximately three times larger than the conventional flexure.[32] Additionally, the split-tube flexure exhibits a fixed axis of rotation (along the long axis of the tube intersecting the links), which enables well-characterized kinematics.

5. SMALL-SCALE MANIPULATOR DESIGN

The split-tube flexure joints have been incorporated into a three degree-of-freedom manipulator that utilizes a direct-drive semi-parallel five-bar linkage revolute configuration. The manipulator is shown in Figures 7 and 8. The five-bar linkage segment is shown in the schematic of Figure 9 and the design drawing of Figure 10. The link lengths of kinematic importance to the manipulator, which are links one and the cantilevered segment of link four as shown in Figure 9, are both 40 mm long, which enable the manipulator to access an approximate cubic workspace of two centimeters to a side with joint ranges of motion of approximately ±15 degrees per joint. As seen in Figure 7, each manipulator revolute joint consists of two split-tube flexures rather than one. The double and single split-tube configurations are referred to as compound and simple configurations, respectively. Arranging the flexures in the compound configuration offers significantly better overall revolute joint behavior. Mechanical analysis shows that the compound configuration exhibits 4 times the revolute stiffness, 64 times the axial stiffness, and 16 times the bending stiffness of the simple joint configuration. A flexure-based revolute joint can be characterized by the ratio of revolute stiffness to axial stiffness and the ratio of revolute stiffness to bending stiffness, both of which would approach zero in the ideal case. Though the absolute value of the revolute stiffness is 4 times larger for the compound ratio, the ratio of revolute to axial stiffness and of revolute to bending stiffness are 16 and 4 times smaller, respectively,
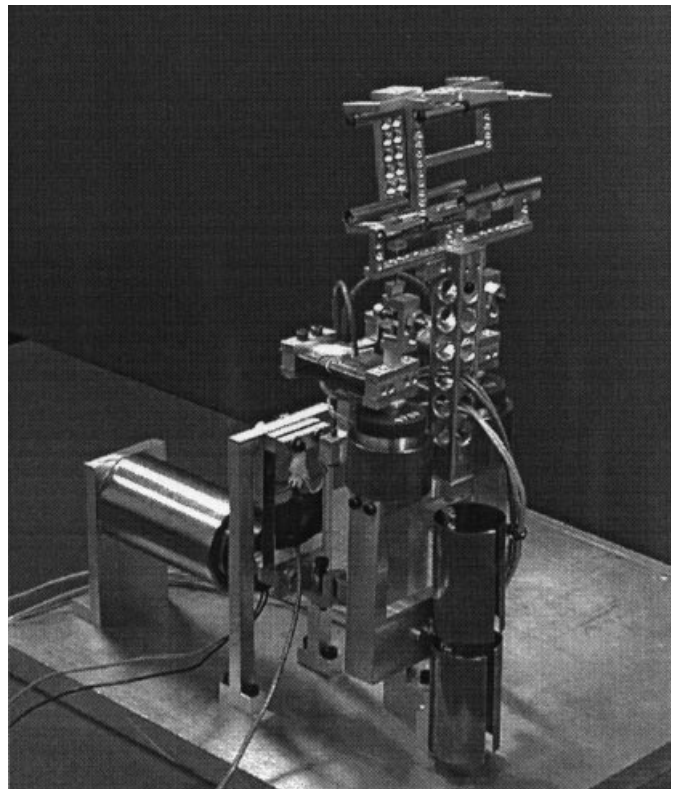

Fig. 7. Three degree-of-freedom compliant-mechanism-based small-scale manipulator.

than the simple joint. The compound joint therefore offers better joint behavior, and thus was selected for the micromanipulator configuration.

Manipulator actuation is provided by voice coil actuators that interface with the manipulator via pre-tensioned push-pull rod mechanisms with knife-edge joints. Specifically, the rods push with knife-edge joints and pull via pre-tensioned cables that are strung through the hollow rods. The actuators are mounted in flexure suspensions, and thus
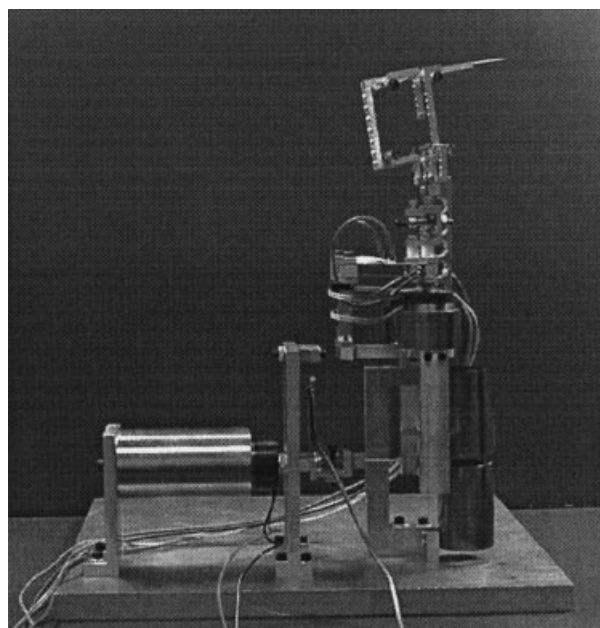

Fig. 8. Side view of the three degree-of-freedom compliant-mechanism-based small-scale manipulator.
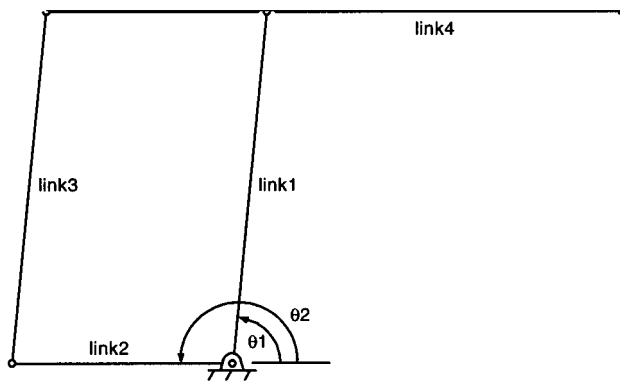
Fig. 9. Kinematic model of five-bar linkage segment of micro-manipulator.

are devoid of stick-slip friction and backlash. The actuator suspensions include strain-gage-based position sensors for collocated position feedback. Note that well-behaved revolute joints are of great import when using sensors in the actuator space, since task-space accuracy is dependent upon well-known kinematic transformations. The actuator suspensions and the push-pull mechanisms are shown in Figures 10 and 11. The five-bar actuators (BEI model LA13–12–000), which are shown in Figure 10, provide a continuous force of seven Newtons over a stroke of approximately six millimeters. The base actuator (BEI model LA15–33–000) provides a continuous force of sixteen Newtons over a stroke of approximately eleven
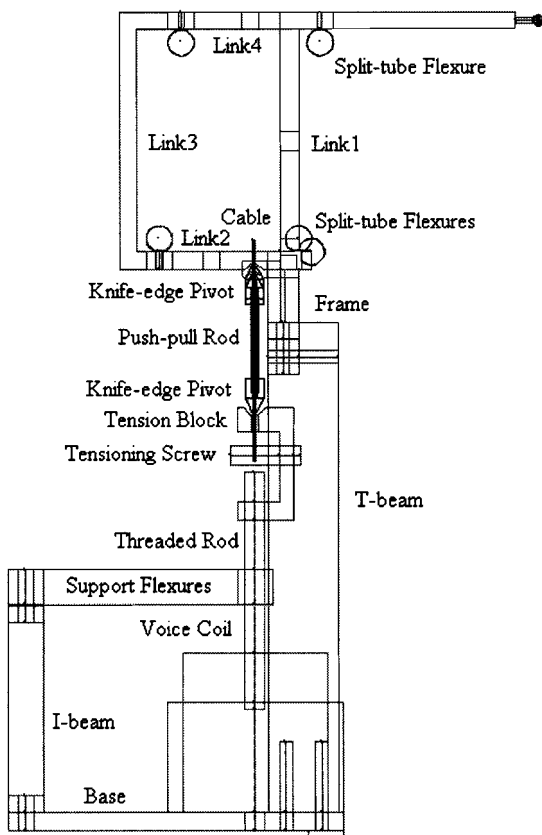

Fig. 10. Side view of the five-bar mechanism showing the voice coil actuators, flexure-based actuator suspensions, and push-pull connecting rods.
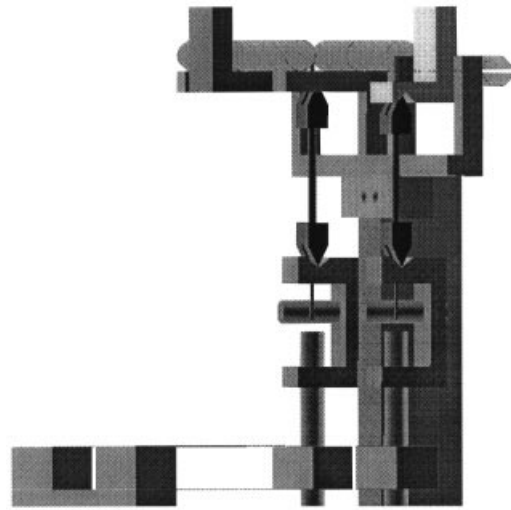

Fig. 11. Solid model of voice coil actuator suspensions and the push-pull mechanisms. The horizontally-oriented pegs that anchor the push-pull rod cable can be turned to pretension the cable and thus eliminate potential backlash.

millimeters. These actuators provide the manipulator with an endpoint force that exceeds 500 milliNewtons in all regions of the workspace (defined by ± 15 degrees of motion per joint).

6. POSITION CONTROLLER DESIGN

Low-level position control of the micromanipulator was implemented with an analog controller as illustrated in the schematic of Figure 12. The input to the controller is the vector of desired actuator displacements, which were computed via inverse kinematics and commanded to the analog controller from a high-level digital controller, which consisted of a 200 MHz Pentium processor with 16-bit A/D and D/A converters. The analog control system utilizes measurement of the voice coil actuator displacements, which are measured by a strain gage bridge on each set of voice coil suspensions, to command the voice coil actuator forces, and thus control manipulator motion. Each joint axis on the manipulator has a corresponding voice coil actuator. The actual displacements that correspond to the θ_1, θ_2 and ϕ joint axes are given by δ_1, δ_2, and δ_3, respectively, and the corresponding actuator forces by F_1, F_2, and F_3. The analog controller is based on using a simple feedback linearization scheme that simplifies the manipulator mechanics to a sufficient extent that independent joint axis controllers can provide effective control of the dynamically coupled manipulator. Specifically, the dynamics relating the three actuator forces to the three actuator displacements are coupled through the joint stiffness and link inertias of the manipulator displacements. The coupling due to the joint stiffnesses is reduced considerably by feedforward terms that effectively cancel the joint stiffnesses. The coupling due to the manipulator link inertias is relatively small, since inertial effects become considerably less significant at small scales, and is thus neglected. Finally, the positional offset generated by gravitational effects on the δ_1 and δ_2 voice coil actuator suspensions are negated by incorporating additional (constant) feedforward terms. As with the inertial

effects of the links, the gravitational effects on the links were considered small (relative to the stiffness effects) and neglected. Given the feedforward stiffness cancellation terms and negligible link inertias, the remaining dynamics were assumed to be sufficiently decoupled to enable single-input single-output compensator design for each actuation axis. Specifically, the remaining dynamics were modeled as decoupled linear second order dynamics for each actuation axis, and a feedback compensator was designed around each to provide stable, high bandwidth tracking. The structure of the low-level analog controller is described in the following two subsections.

6.1 Stiffness compensation
As previously mentioned, the low-level analog controller contains a feedforward term for joint stiffness cancellation. Unlike a conventional robot manipulator, the compliant-mechanism-based micromanipulator is a lightly-damped structure. The purpose of the feedforward stiffness cancellation is to cancel the structural stiffness (i.e., negate the stiffness at each joint), thus rendering the manipulator a metastable mechanism that, in the absence of gravity, remains in any position in which it is placed. The structural stiffness of the manipulator results from two primary components. One component is from the actuator suspensions (linear flexures), and the other is from the manipulator joints (angular flexures). Both stiffnesses are fairly linear, but the joint stiffnesses are reflected to the actuators through the mildly nonlinear transmission of the push-pull rod mechanisms, and thus appear in the actuator space as mildly nonlinear terms. The stiffness cancellation, which consists of linear terms, is therefore effective for small actuator displacements, but becomes less effective toward the edges

of the workspace, where the kinematic nonlinearities introduced by the linkage become more pronounced. This effect is partially compensated by the feedback compensator described in the subsection that follows.

Also, as previously mentioned, an additional purpose of the stiffness cancellation is to decouple the actuation axes. Specifically, the θ_1 and θ_2 axes are coupled by the joint stiffnesses of the five-bar linkage. As shown in the controller schematic of Figure 12, the θ_1/θ_2 coupling is included in the feedforward stiffness cancellation, which in turn significantly diminishes the coupling between the two axes.

6.2 Feedback compensator design
The feedback controller was designed by assuming that, in the presence of the previously described feedforward terms, each manipulator axis is decoupled from the others and exhibits linear second-order dynamics as given by:

$$m_i \ddot{\delta}_i + b_i \dot{\delta}_i + k_i \delta_i = F_i \qquad (6)$$

where δ_i is the actuator displacement and m_i, b_i, k_i, and F_i are the model parameters (mass, damping, and stiffness) and actuator force, respectively, of the ith axis. The model parameters for each axis were determined experimentally by separately measuring the force/displacement relationship and the homogeneous dynamic response. Originally, a proportional-derivative controller was implemented, where the derivative operator was an ideal derivative operator in series with a second-order low pass filter. Specifically, the controller had the form:

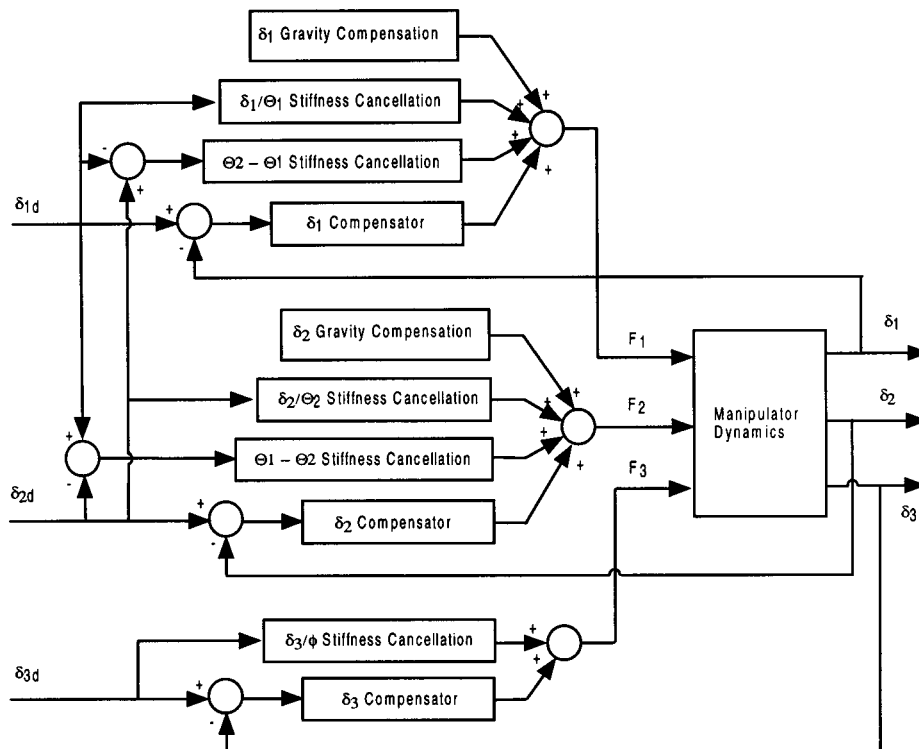$$\frac{F_i(s)}{E_i(s)} = k_{pi} + k_{di}\frac{s}{(\tau s + 1)^2} \qquad (7)$$

Fig. 12. Block diagram of three degree-of-freedom low-level analog position controller.

where F_i and E_i are the Laplace transforms of the actuator force and the actuator displacement error, respectively, for the ith axis, s is the Laplace operator, k_{pi} is the proportional gain, k_{di} the derivative gain, and τ determines the cutoff frequency of the low pass filter. This controller failed to provide adequate performance. Specifically, the closed-loop system exhibited unstable behavior at fairly low gains. As a result, a model-based compensator of the following form was designed using root locus techniques to provide stable behavior at higher gains and thus enable high bandwidth tracking:

$$\frac{F_i(s)}{E_i(s)} = k_p + k_d \frac{(s+a_i)(s+b_i)}{(s+c_i)(s+d_i)} \qquad (8)$$

where a_i, b_i, c_i and d_i determine the locations of the compensator zeros and poles for the ith actuation axis. Specifically, this control structure enabled a choice of zero and pole locations such that the closed-loop system was stable, with the dominant poles exhibiting a damping ratio of approximately $\zeta = 0.7$.

7. PERFORMANCE CHARACTERIZATION

7.1 Smoothness and positioning resolution
Experiments were conducted to demonstrate the absence of backlash and frictional effects in the manipulator behavior. Specifically, sinusoidal trajectories were commanded through space that required reversals of all actuators and all kinematic joints. The endpoint motion of the manipulator was measured directly with a laser displacement sensor (Polytech PI model OFV2200/OFV511) to detect the presence of backlash and friction in the manipulator. The absence of gross discontinuities and the lack of geometric irregularities in the measured sinusoidal trajectories in turn indicated the absence of hard nonlinearities in the manipulator behavior. This qualitative approach to the detection of hard nonlinearities is similar to that used by Morel and Dubowsky.[33] Additionally, to better isolate and detect the presence of backlash and Coulomb friction, the trajectories were drawn quasistatically to avoid inertial filtering, and the laser displacement data was left unfiltered.

Figure 13 shows the prototype spatial sinusoidal trajectory used to evaluate manipulator smoothness, together with its Cartesian components. Figures 14 and 15 show the unfiltered position data for 0.25 Hz sinusoidal trajectories with 9.5 mm and 1.3 mm peak-to-peak amplitudes, respectively. Both figures indicate a lack of gross discontinuities, and therefore are indicative of the absence of significant backlash and Coulomb friction effects. Figure 16 through 18 show the unfiltered position data for 0.10 Hz sinusoidal trajectories with 120 μm, 65 μm, and 25 μm peak-to-peak amplitudes, respectively. The absence of gross irregularities in the sinusoidal paths indicate the manipulator mechanics are not significantly influenced by backlash or Coulomb friction. At these scales, however, the presence of sensor noise (approximately one to two microns, peak-to-peak) prevents definitive assertions regarding the complete absence of these physical hard nonlinearities. This level of

noise could be reduced by low-pass filtering, but as previously stated, such filtering was avoided to prevent masking of any physical hard nonlinearities.

7.2 Tracking performance at higher speeds
An indication of manipulator bandwidth is demonstrated in the data of Figure 19, which shows the commanded and actual trajectories for a 10 mm diameter circle drawn at
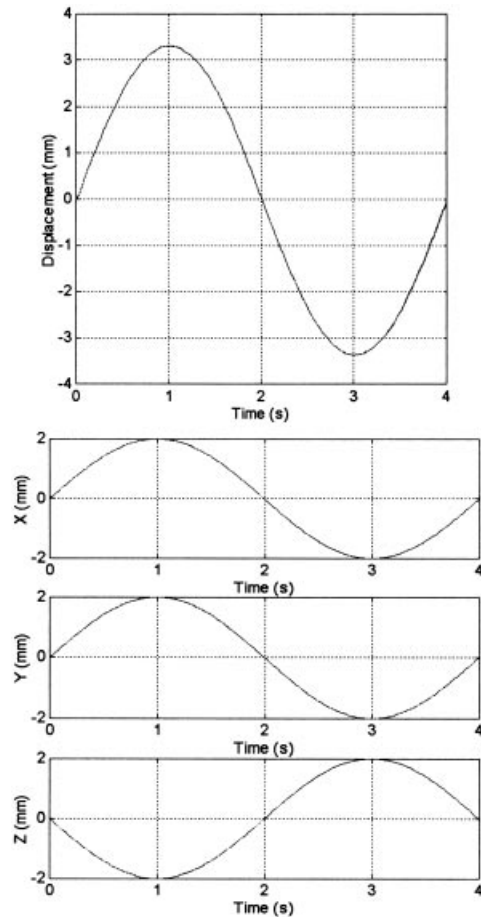

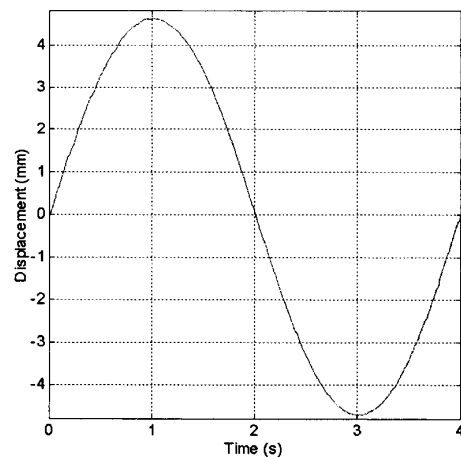Fig. 13. Sinusoidal trajectory (top) and corresponding Cartesian component motions (bottom three plots).

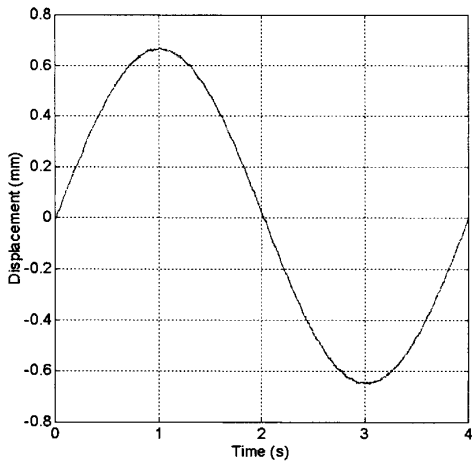Fig. 14. Unfiltered data showing a 9 mm peak-to-peak sinusoidal motion at 0.25 Hz.

Fig. 15. Unfiltered data showing a 1.3 mm peak-to-peak sinusoidal motion at 0.25 Hz.

5.0 Hz, and also shows the corresponding *x*-axis and *y*-axis component motions. The *x*-axis and *y*-axis trajectories (shown as a function of time) demonstrate that no significant phase lag is present at this tracking frequency, which indicates that at 5.0 Hz the manipulator is not approaching a phase-related bandwidth limitation.
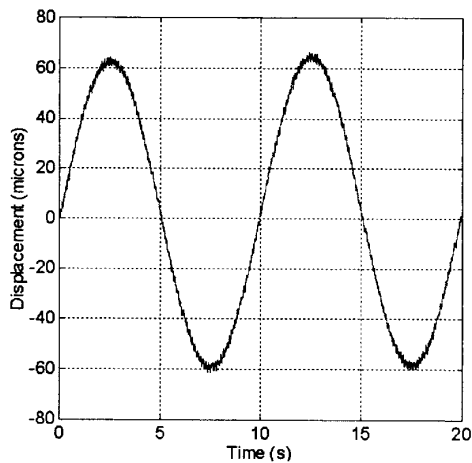

Fig. 16. Unfiltered data showing a 120 micron peak-to-peak sinusoidal motion at 0.1 Hz.
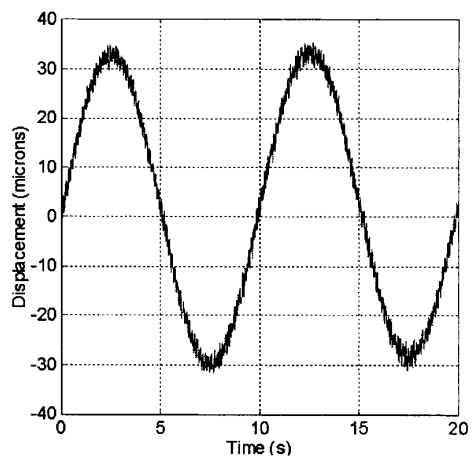

Fig. 17. Unfiltered data showing a 65 micron peak-to-peak sinusoidal motion at 0.1 Hz.
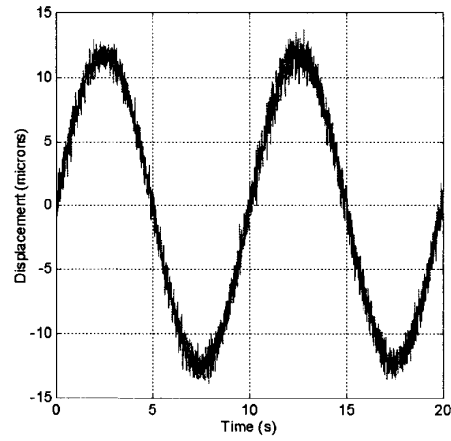

Fig. 18. Unfiltered data showing a 25 micron peak-to-peak sinusoidal motion at 0.1 Hz.

8. CONCLUSION
A three degree-of-freedom compliant-mechanism-based micromanipulator has been developed for precision manipulation of small-scale environments. Incorporation of a unique flexure joint enables a significant range of motion
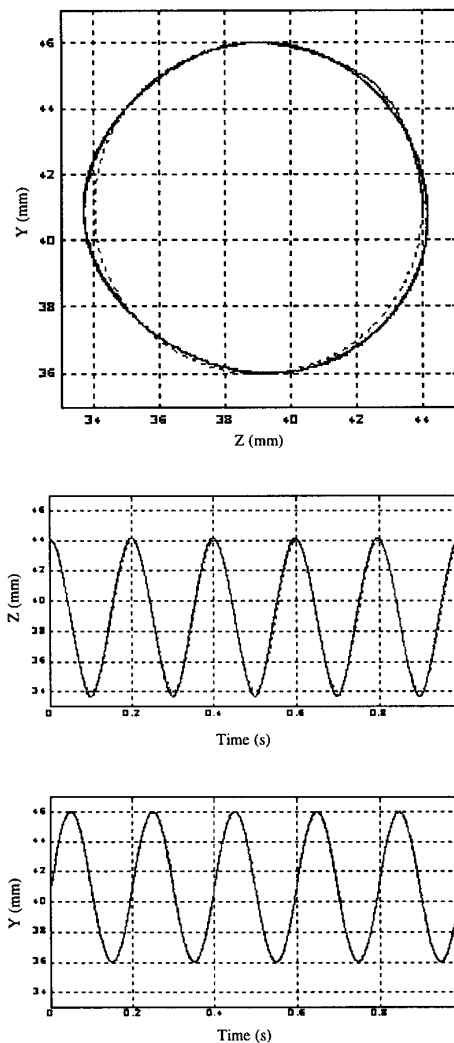

Fig. 19. Five revolutions of a 10 mm diameter circle at 5 Hz. Some magnitude error is evident in the tracking, but nearly zero phase lag indicates the manipulator is not approaching bandwidth limitations.

and well-behaved kinematic properties. Experiments indicate that the manipulator exhibits no measurable backlash or stick-slip behavior, and thus presents no fundamental physical limitations on position or force resolution.

References
1. C.H. An and J.M. Hollerbach, Dynamic stability issues in force control of manipulators," *Proceedings of the IEEE International Conference on Robotics and Automation* (1987), pp. 890–896.
2. J.E. Colgate and N. Hogan, "Robust control of dynamically interacting systems" *Int. J. Control* **48**(1), 65–88 (1988).
3. S.D. Eppinger and W. Seering, "On dynamic models of robot force control," *Proceedings of the IEEE International Conference on Robotics and Automation* (1986) pp. 29–34.
4. H. Kazerooni, "Contact instability of the direct drive robot when constrained by a rigid environment" *IEEE Transactions on Automatic Control* **35**(6), 710–714 (1990).
5. N.G. Chalhoub and A.G. Ulsoy, "Effect of a self-locking drive mechanism on the performance of a flexible robot arm" *Proceedings of the American Control Conference* (1990) pp. 1270–1271.
6. A. Gogoussis and M. Donath, "Determining the effects of Coulomb friction on the dynamics of bearings and transmission in robot mechanisms" *ASME Journal of Mechanical Design* **115**(2), 231–240 (1993).
7. E.S. Nakagawa, Y. Uretake and Z. Cai, Vibration analysis of robot manipulators: the effect of backlash in transmission mechanisms" *Transactions of the Japan Society of Mechanical Engineers* **57**(544), 3877–3881 (1991).
8. H. Schempt and D.R. Yoerger, "Study of dominant performance characteristics in robot transmissions" *ASME Journal of Mechnical Design,* **115**(3), 472–482 (1993).
9. W.T. Townsend and J.K. Salisbury, "The effect of Coulomb friction and stiction on force control" *Proceedings of the IEEE Conference on Robotics and Automation* (1987) pp. 883–889.
10. H. Asada and K. Youcef-Toumi, *Direct-Drive Robots: Theory and Practice* (MIT Press, Cambridge, Massachusetts, 1987).
11. R. Fearing, "Survey of sticking effects for micro parts handling" *Proceedings of the IEEE/RSJ Conference on Intelligent Robots and Systems* **2**, 212–217 (1995).
12. W. Trimmer and R. Jebens, "Actuators for micro robots" *Proceedings of the IEEE International Conference on Robotics and Automation* (1989) pp. 1547–1552.
13. W. Trimmer, "Microrobots and micromechanical systems" *Sensors and Actuators* **19**, 267–287 (1989).
14. I.W. Hunter, S. Lafontaine, P.M.F. Nielsen, P.J. Hunter and J.M. Hollerbach, "Manipulation and dynamic mechanical testing of microscopic objects using a tele-micro-robot system" *IEEE Control Systems Magazine* 3–9 (February, 1990).
15. I.W. Hunter, D.D. Tilemachos, S.R. Lafontaine, P.G. Charette, L.A. Jones, M.A. Sagar, G.D. Mallinson and P.J. Hunter "A

16. teleoperated microsurgical robot and associated virtual environments for eye surgery" *Presence* **2**(4), 265–280 (1994).
16. B. Hannaford, A. Bejczy, P. Buttolo, M. Moreyra and S. Venema, "Mini-teleoperation for space research" *Proceedings of the International Symposium on Microsystems, Intelligent Materials and Robots* (September 1995) pp. 524–527.
17. P.S. Jensen, M.R. Glucksberg, J.E. Colgate, K.W. Grace and R. Attariwala, "Robotic micromanipulator for ophthalmic surgery" *Proceedings of the First International Symposium on Medical Robotics and Computer-Assisted Srugery* (1994) **Vol. 2**, pp. 204–210.
18. R.L. Hollis, S. Salcudean and D.W. Abraham, "Toward a tele-nanorobotic manipulation system with atomic scale force feedback and motion resolution" *Proceedings of the IEEE Micro Electro Mechanical Systems* (1990) pp. 115–119.
19. S.E. Salcudean and J. Yan, "Towards a Force-Reflecting Motion-Scaling System for Microsurgery" *Proceedings of the IEEE International Conference on Robotics and Automation* (1994) pp. 2296–2301.
20. R.L. Hollis and S.E. Salcudean, "Design and control of a motion scaling system for microsurgery experiments" *Proceedings of the First International Symposium on Medical Robotics and Computer-Assisted Surgery* (1994) **Vol. 2**, pp. 211–216.
21. S.E. Salcudean, N.M. Wong and R.L. Hollis, "Design and control of a force-reflecting teleoperation system with magnetically levitated master and wrist" *IEEE Transactions on Robotics and Automation* **11**(6), 844–858 (1995).
22. T. Fukuda, M. Fujiyoshi, F. Arai and H. Matsuura, "Design and dextrous control of micromanipulator with 6 D.O.F." *Proceedings of the IEEE International Conference on Robotics and Automation* (1991), pp. 1628–1633.
23. P. Kallio, M. Lind, Q. Zhou and H. Koivo, "A 3 DOF piezohydraulic parallel micromanipulator" *Proceedings of the IEEE International Conference on Robotics and Automation* (1998) pp. 1823–1828.
24. *NASA Tech Briefs* "Small surgery, big results" 16–17 (November 1994).
25. J. Paros and L. Weisbord, "How to design flexure hinges" *Machine Design* **37**(27), 151–156 (1995).
26. K. Ragulskis, M. Arutunian, A. Kockikian and M. Pogosian, "A study of fillet type flexure hinges and their optimal design" *Vibration Engineering* 447–452 (1989).
27. L.L. Howell and A. Midha, "A method for the design of compliant mechanisms with small-lenge flexural pivots" *ASME Journal of Mechanical Design* **116**(1), 280–290 (1994).
28. L.L. Howell, and A. Hidha, "Parametric deflection approximations for end-loaded, large-deflection beams in compliant mechanisms" *ASME Journal of Mechanical Design* **117**(1), 156–165 (1995).
29. L.L. Howell and A. Midha, "A loop-closure theory for the analysis and synthesis of compliant mechanisms" *ASME Journal of Mechnical Design* **118**(1), 121–125 (1996).
30. M. Goldfarb and N.Celanovic, "A flexure-based gripper for small-scale manipulation" *Robotica* **17**(2), 181–188 (1999).
31. J.P. Den Hartog, *Advanced Strength of Materials* (McGraw-Hill, New York, 1952) pp. 10–17.
32. M. Goldvarb and J. Speich, "Eliminating non-smooth non-linearities with compliant manipulator design", *Proceedings of the American Control Conference* (1998) pp. 2118–2122.
33. G. Morel and S. Dubowsky, "The precise control of manipulators with joint friction: a base force/torque sensor method" *Proceedings of the IEEE Conference on Robotics and Autoamtion* (1996) pp. 360–365.